Energy Proceedings
Vol 50, 2025
ISSN 2004-2965

The Effect of Solvated Ionomers on Coating Appearance in Wet Process Electrode of PEMFC#

Daozeng Yang, Bing Li*, Daijun Yang, Pingwen Ming, Cunman Zhang
Affiliation of author: School of Automotive Studies and Clean Energy Automotive Engineering Center, Tongji University, Shanghai, 201804, China
(Corresponding Author E-mail: libing210@tongji.edu.cn)

ABSTRACT

In the realm of wet process electrode development for Proton Exchange Membrane Fuel Cells (PEMFCs), the rheological characteristics of the catalyst slurry play a pivotal role in shaping the coating appearance. The intricate interplay between solvated ionomers and catalysts gives rise to diverse and complex interactions, which in turn exert specific functions on aggregates, thus influencing the fluid properties significantly. This investigation utilizes rheological assessments to scrutinize the fluctuations in shear viscosity, viscoelastic behavior, and thixotropic properties of various water/alcohol slurries. The findings suggest that ethanol molecules, with their higher polarity, augment the surface potential of slurry aggregates, concomitantly diminishing slurry viscosity and compromising coating uniformity. This, however, leads to surface imperfections while enhancing the polarization efficiency of the membrane electrodes under high current densities, elevating the voltage output from 0.624V to 0.646V at 2A cm^{-2}. Conversely, n-propanol molecules, relatively less polar, intensify the slurry's viscosity and ameliorate surface flaws in the coating, thereby reducing the extra-large pore, exhibiting elevated polarization voltage at lower current densities, raising the voltage from 0.851V to 0.866V at 0.2A cm^{-2}.

Keywords: PEMFC, Catalyst slurry, Rheology, Coating appearance, Extra-large pore

NONMENCLATURE

Abbreviations	
PEMFC	Proton Exchange Membrane Fuel Cell
MEA	Membrane Electrode Assembly
I/C ratio	The mass ratio of ionomer to the carbon support
CCM	Catalyst coated membrane
EW	Equivalent mass
ET	Ethanol
NPA	n-propanol
Symbols	
G’	Storage modulus (Pa)
G”	Loss modulus (Pa)

1. INTRODUCTION

Proton exchange membrane fuel cells (PEMFCs) represent a crucial technology that converts chemical energy into electrical energy, demonstrating sustainability, zero carbon emissions, and higher energy conversion efficiency[1, 2]. They play a pivotal role in tackling the increasing energy dilemmas faced globally. Due to cost and scale limitations, the global adoption and application of fuel cells are currently proceeding at a relatively slow pace[3, 4]. In the context of large-scale industrial manufacturing, catalytic layers, being fundamental constituents of fuel cells, are typically fabricated utilizing wet coating methodologies[5]. The rheological attributes and other physical characteristics of the catalyst slurry, acting as the precursor to catalytic layers, hold considerable sway over the appearance and structure of the coating[6, 7].

Compared to the catalyst dispersion used in the spraying process (<1.0 wt.%)[8], the catalyst slurry required for wet coating has a higher solid content (>10.0 wt.%)[5]. Typically, when formulating catalyst slurry, many researchers commonly utilize the mass ratio of ionomer to the carbon support in the catalyst (I/C ratio) as key parameters[9]. As an ionic polymer, Nafion exhibits both hydrophilic and hydrophobic properties, which adsorb onto catalyst particles and provide electrostatic forces and steric hindrance, preventing particle agglomeration in the dispersion[10, 11]. Agglomerated catalyst particles can lead to slurry coating interrupts, leaks, and bubbles during the coating process, and result in defects such as pinholes and cracks in the catalytic layer[12, 13]. The microstructure of the catalytic

This is a paper for the 16th International Conference on Applied Energy (ICAE2024), Sep. 1-5, 2024, Niigata, Japan.

layer is composed of the aggregates within the slurry, and the structure of these aggregates is related to the ionomer and the catalyst support. Welch et al.[14] examined the ionomer morphology in various solvents, discovering that they adopt a tightly packed rod-like structure in solutions with high dielectric constants. Concurrently, Ngo et al.[15] explored the ionomer morphology in diverse water-alcohol mixed solvents, revealing that in water-rich mixtures, the ionomer structure was more compact and exhibited reduced particle size. Moreover, as the dielectric constant of the mixed solvents increased, the catalytic layer demonstrated a larger electrochemically active surface area. Li et al.[16] developed two types of carbon support capable of generating positive and negative surface potentials in solvents, respectively, by modifying surface functional groups. This modification modulated the interaction between ionomers and the carbon support, expanded the pore structure within the catalytic layer, and minimized mass transport resistance[16, 17]. Consequently, studying the properties of ionomers after solvation is crucial for optimizing slurry characteristics and coating architectures[14].

Therefore, we modify the zeta potential on the surfaces of ionomer aggregates and their hydrodynamic diameter within the solvent by adjusting the solvent composition, aiming to achieve ionomer dispersions with varied morphological structures. Additionally, we investigate the charge distribution characteristics on the surface of carbon carriers in the solvent and examine the relationship between the interactions between ionomer aggregates and carbon support and their impact on the rheological properties of the slurry. By conducting tests for shear stress, viscoelasticity, and thixotropy, we acquired insights into the network structural characteristics among aggregates within the slurry. The microstructure and pore structure of the catalytic layer were analyzed using SEM, FIB-TEM, elemental mapping, and MIP, and its polarization performance was evaluated through electrochemical tests.

2. EXPERIMENTS AND METHODS

Deionized water, n-propanol, and ethanol were used as solvents, with Nafion (EW=1100) serving as the dispersant, and a Pt/C catalyst (LongSun, 50 wt.%) was employed to prepare the slurry. The slurry had a designed solid content of 10 wt.%, with a mass ratio of 7:3 for water to alcohol component, and the ethanol concentrations in the alcohol component were adjusted to 1/3, 2/3, and 3/3, respectively, resulting in three distinct sample groups. A planetary ball mill (MAZERUSTER, KK-400WE) was utilized for slurry homogenization, operating at both orbital and rotational speeds of 576 RPM for 45 min, to produce the catalyst slurry. The catalytic layer was fabricated using slot coating, with a gap of 150 μm and a coating rate of 40 mm/s. By regulating the flow rate, coatings were produced with Pt loadings of 0.1 mg_{Pt} cm^{-2} for the anode and 0.3 mg_{Pt} cm^{-2} for the cathode. Following the preparation of the catalyst coated membrane (CCM) via a thermal transfer method, carbon paper was hot-pressed onto the anode and cathode catalytic layers to create the Membrane Electrode Assembly (MEA).

The pH and zeta potential, particle size, and rheological properties of the dispersion were measured using particle potential titrator (Colloid Metrix, Stabino), nanoparticle size analyzer (Nano-flexII, Colloid Metrix), and rotational rheometer (Anton Paar, MCR302), respectively. The surface functional groups of the carbon carrier were analyzed with an infrared analyzer. The surface and cross-section of the coating were examined using a scanning electron microscope (SEM) and a transmission electron microscope (TEM). Elemental mapping was used to analyze the elemental composition of the sample cross-section. The pore structure of the sample was assessed using mercury intrusion porosimetry. The single-cell polarization curve was tested using the fuel cell test platform (Greenlight, G20). The samples were activated for 6 h at 75°C, 60% relative humidity, with anode and cathode pressures of 0.8 MPa and 1.2 MPa, respectively, and a voltage of 0.3 V. During the test, the anode and cathode pressures were set to 1.5 MPa and 1.7 MPa, respectively, and stable readings were recorded after the current was applied.

3. RESULTS AND DISCUSSION

Initially, the zeta potential and hydrodynamic diameter of the ionomer dispersion were assessed. The surface zeta potential of ionomer aggregates significantly increases with higher ethanol concentrations in the alcohol component (Figure 1a).

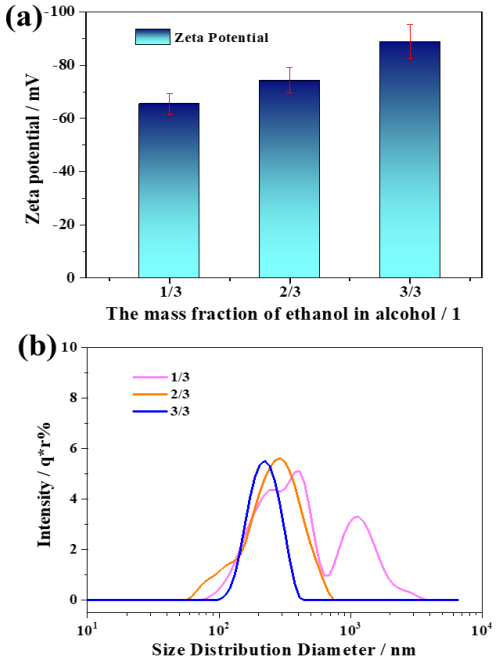

Figure 1. Measurement of zeta potential and hydrodynamic diameter of ionomer dispersion with ethanol mass accounting for 1/3, 2/3 and 3/3 of alcohols component, respectively. (a) Zeta potential, (b) Hydrodynamic diameter

The ionomer dispersion was diluted to 0.1 wt% for dynamic light scattering, revealing that increased ethanol content in the solvent reduced the hydrodynamic diameter of ionomer aggregates from approximately 600 nm to around 250 nm. However, the solvent was depleted of agglomerated particles smaller than 60-100 nm (Figure 1b). This demonstrates that in a water/ethanol/n-propanol composite solvent, enhancing ethanol content favorably results in smaller ionomer dispersions.

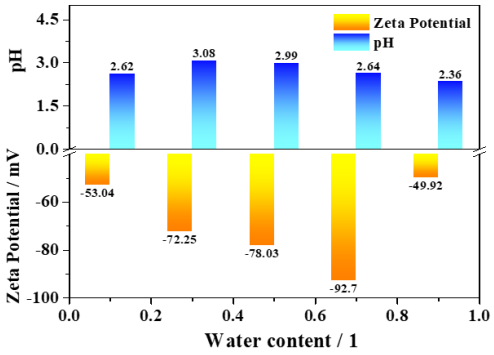

Figure 2. Zeta potential and pH test of carbon suspension with water/ethanol solvent.

Subsequently, the carbon carrier dispersion was examined. In the water/ethanol mixture, both the zeta potential and pH of the carbon dispersion exhibited an initial increase followed by a decrease as the water content rose. At a water content of 0.3, the pH of the carbon suspension reached its maximum, while at 0.7, the Zeta potential of the suspension became the most negative (see Figure 2). The findings indicate that an optimal increase in water content within the carbon suspension enhances the Zeta potential strength of the aggregates and promotes the formation of more Lewis acids. However, an increase in water content diminishes the solvent's ability to wet the carbon carrier, leading to an increase in the agglomeration of carbon carrier particles. The presence of -SO_3H groups on the carbon carrier generate -SO_3^- and H^+ in the solvent, leading to a negative surface potential on the aggregates and imparting an acidic character to the dispersion.

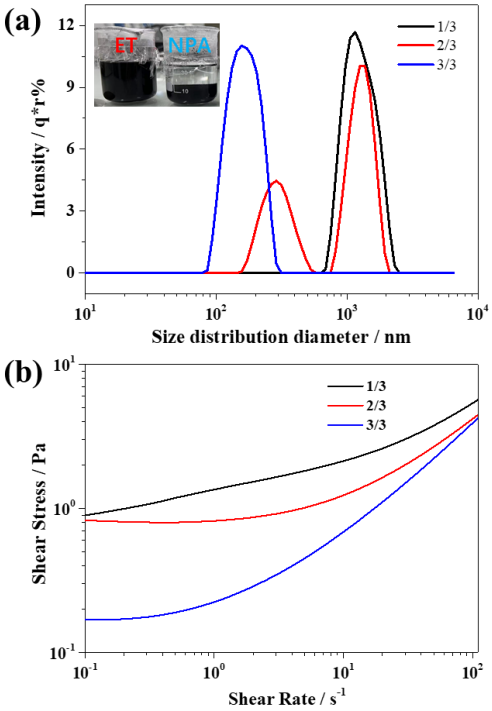

Figure 3. (a) Hydrodynamic diameter test of carbon carrier with ethanol mass accounting for 1/3, 2/3 and 3/3 of alcohols component respectively, (b) shear stress test of catalyst slurry with ethanol mass accounting for 1/3, 2/3 and 3/3 of alcohols component respectively

Further, we found significant differences in the behavior of this type of carbon carrier in ethanol and n-propanol solvents. Without the addition of ionomer, the carbon carrier exhibits a large hydrodynamic diameter in a water/ethanol/n-propanol mixed solvent. When mass radio of ethanol to alcohols reach 1/3, the carbon carrier particles are predominantly micron-sized. With the mass ratio reach to 2/3, the diameter of the carrier particles reduces, though the solvent still contains many micron-sized particles. However, the carbon carrier particles can

be uniformly dispersed in water/ethanol solvent, reducing the hydrodynamic diameter of the carbon carrier to less than 200 nm. Direct observation showed that after the carbon carrier was dispersed in n-propanol, solid-liquid separation occurred upon overnight placement, indicating that n-propanol was not conducive to the dispersion of the carrier (Figure 3a).

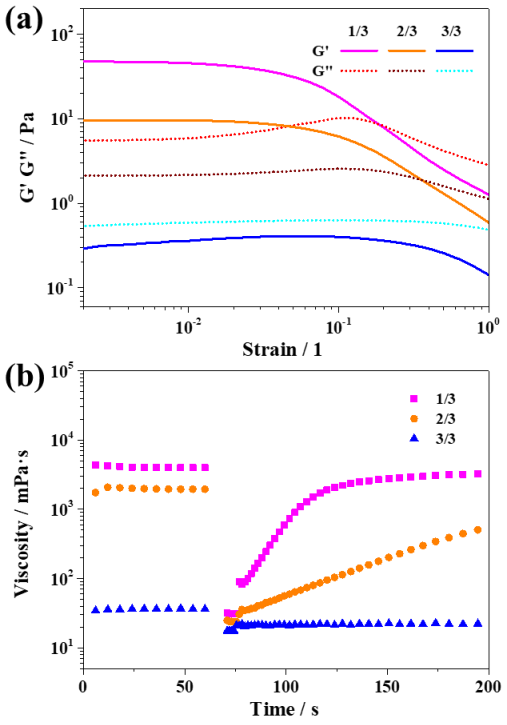

Figure 4. Viscoelasticity and thixotropy test of catalyst slurry with ethanol mass accounting for 1/3, 2/3 and 3/3 of alcohols component respectively, (a) Viscoelasticity test, where G 'stands for storage modulus, and G' is the apparent loss modulus, (b) Thixotropy test, with shear rate of 0.1s^{-1} in the first stage, simulating the static state of slurry; In the second stage, the shear rate was 100 s^{-1}, simulating the damage state of slurry structure; In the third stage, the shear rate was 0.1s^{-1}, simulating the automatic recovery of slurry structure

After adding ionomer, rheological testing was conducted on the slurry. The test results revealed that the slurry with ethanol making up 1/3 of the alcohols solvent exhibited the highest shear stress (0.1s^{-1}), suggesting the formation of a network structure within the slurry. As the mass ratio increased to 2/3, the slurry's shear stress fell below 0.2 Pa, indicating minimal connectivity among the aggregates and greater dispersion (Figure 3b). Consequently, both the ionomer and catalyst particles in the slurry possess surfaces with a negative electrical charge. The presence of electrostatic forces between these negatively charged particles impedes the ionomer's full adsorption onto the catalyst aggregates.

The slurry's viscoelasticity and thixotropy were tested. The test results revealed that as the ethanol content in the alcohols component increased, the network strength between aggregates in the slurry began to decrease, along with a reduction in the storage modulus G' of the slurry. When the ethanol' mass ratio in alcohols reaches 3/3, the slurry's loss modulus G" becomes greater than its storage modulus, indicating the absence of a structural framework between the aggregates. The thixotropy test demonstrated that all three types of slurries exhibit significant thixotropy. For slurries with a higher storage modulus, the viscosity can recover within 50 s after shearing at a rate of 100 s^{-1}, suggesting re-establishment of the particle structure. In contrast, slurries with a lower storage modulus exhibit difficulty in viscosity recovery post-shearing, indicating partial particle dispersion and fragmentation under shear stress, making reassembly in a short time frame challenging.

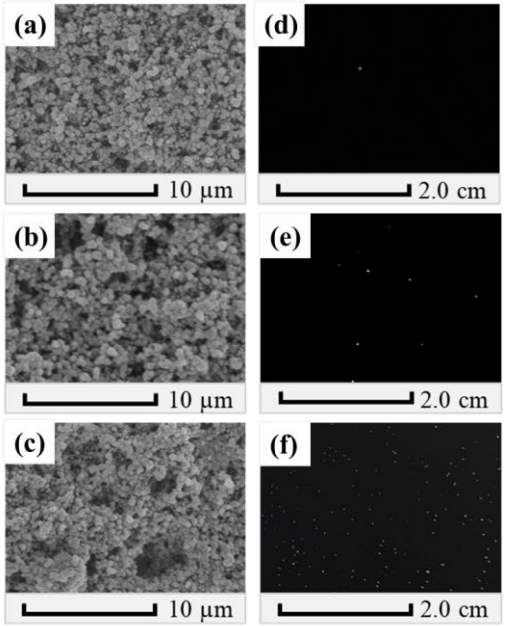

Figure 5. SEM and photos of catalyst slurry coating with ethanol mass accounting for 1/3, 2/3 and 3/3 of alcohols component respectively. (a&d) 1/3, (b&e) 2/3, (c&f) 3/3

To investigate the influence of interactions between two types of negatively charged carbon particles on coating morphology, the coating surface was examined using optical equipment. SEM analysis revealed that coatings formed from slurries with an ethanol mass ratio of 1/3 in alcohols component exhibited smoother surfaces with fewer large aggregate particles. As the ethanol mass ratio increased to 2/3 and 3/3, the coating

surfaces became uneven and developed micron-sized macropores. Photographs of the coatings taken against a white light plate showed that as the ethanol content increased, more translucent holes began to appear on the coating surface. Particularly for the coating using a slurry with an ethanol mass ratio of 3/3 in alcohols solvent, these holes uniformly distributed across the entire field of view. This indicates that during the drying and coating formation process, catalyst aggregates composed of two types of negatively charged particles, unhindered by a network structure, will undergo solvent stripping and aggregation, leading to an increase in defects.

To observe the effect of interactions between ionomer aggregates and catalyst aggregates on the coating's nanostructure at the microscopic level, the cross-section of the catalytic layer was examined using TEM. It was observed that when the ethanol mass ratio in alcohols solvent was 1/3, the catalyst aggregates interconnected, forming a dense aggregate structure. As the ethanol mass ratio increased to 2/3, distinct boundaries between aggregates became evident. When the ethanol mass ratio reached 3/3, the aggregate structure became more porous, with increased interparticle voids.

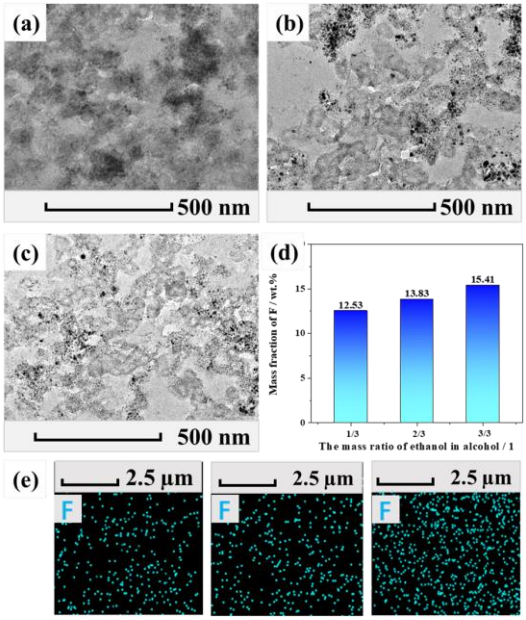

Figure 6. (a), (b), (c) TEM images of the cross-sections of catalyst slurry coatings with ethanol mass ratio of is 1/3, 2/3, 3/3 in alcohol component, (d) normalized mass fraction of the F element on the coating surface, (e) F elemental mapping of the coating surface

SEM elemental mapping was employed to examine the surface of the catalytic layer. Results indicated that with increasing ethanol content, the fluorine (F) elemental composition on the catalytic layer surface rose from 12.53 wt.% to 15.41 wt.%, suggesting heightened ionomer migration to the coating surface during the slurry wet coating drying process. The migration of ionomer to the coating surface can be attributed to two factors: firstly, the negatively charged surfaces of catalyst carbon particles and ionomer hinder stable adsorption of the ionomer on the surfaces of catalyst aggregates; secondly, the structural integrity among particles in slurries with lower viscosity is minimal, facilitating easier movement of ionomer molecules within the solvent.

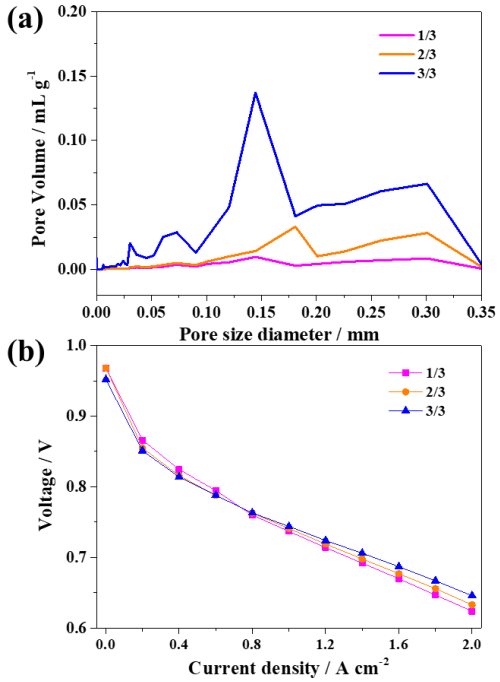

Figure 7. (a)Pore size distribution curve, and (b)Polarization curve of catalyst slurry coating with ethanol mass accounting for 1/3, 2/3 and 3/3 of alcohols component respectively

The coating's pore size distribution was examined using a mercury porosimeter, revealing that at an ethanol mass ratio of 1/3 in the alcohol component, the coating had minimal macro-porous structures; however, at a ratio of 2/3, pores larger than 0.15 mm started to emerge; and at 3/3, the coating's large pore volume surged, correlating with the numerous transparent pores evident on its surface. Consequently, while ethanol solvent enriches the pore structure of coatings, it primarily leads to an increase in defects. Additionally, electrochemical testing was conducted to assess the coating's polarization performance. The findings indicated that at lower current densities, higher ethanol content resulted in lower voltages. As current density

increased to 0.8A cm^{-2}, the rate of voltage drop decelerated, leading to higher voltages observed in the high current density range.

4. CONCLUSIONS

(1) An increase in ethanol content within water/alcohol composite solvents results in smaller ionomer agglomerate particles and a higher Zeta potential. Additionally, within a solvent containing 0.7 water content, the carbon carrier exhibits an elevated Zeta potential. The interaction between two negatively charged agglomerate particles leads to a reduction in slurry viscosity and a thorough disruption of the network structure among catalyst agglomerates.

(2) During the drying process, the feeble interparticle network structure prevents the reduction of thermal motion, leading to the formation of numerous extra-large pore structures in the dried coating.

(3) The appearance of extra-large pore means that the solid region inside the coating which can be used as a reaction three-phase interface is replaced by the gas phase, which reduces the polarization voltage at low current density (<0.8mA cm^{-2}). However, the extra-large pores are conducive to the transmission of water and gas, and to the improvement of reaction kinetics at high current density.

ACKNOWLEDGEMENT

The authors appreciate the Program of Ministry of Science & Technology of China (No. 2022YFB2502504) for financial support.

REFERENCE

[1] Li J-C, Xu H, Zhou K, Li J-Q. A review on the research progress and application of compressed hydrogen in the marine hydrogen fuel cell power system. Heliyon. 2024;10.

[2] Cai F, Cai S, Tu Z. Proton exchange membrane fuel cell (PEMFC) operation in high current density (HCD): Problem, progress and perspective. Energy Conversion and Management. 2024;307.

[3] Wang Y-C, Huang W, Wan L-Y, Yang J, Xie R-J, Zheng Y-P, et al. Identification of the active triple-phase boundary of a non-Pt catalyst layer in fuel cells. Science Advances. 2022;8.

[4] Osman AI, Chen L, Yang M, Msigwa G, Farghali M, Fawzy S, et al. Cost, environmental impact, and resilience of renewable energy under a changing climate: a review. Environmental Chemistry Letters. 2022;21:741-64.

[5] Ren H, Meng X, Lin Y, Li X, Shao Z. Surface enrichment of ionomer in fuel cell catalyst layer prepared using slot-die coating method. Journal of Power Sources. 2023;580.

[6] Woo SH, Kim S, Woo S, Park S-H, Kang YS, Jung N, et al. Investigating the effect of solvent composition on ink structure and crack formation in polymer electrolyte membrane fuel cell catalyst layers. Korean Journal of Chemical Engineering. 2023;231:529-38.

[7] Yoshimune W, Harada M. Temperature-induced shear-thinning in catalyst inks. Electrochemistry Communications. 2021;130.

[8] Inaba M, Kamitaka Y, Kodama K. Eliminating the need for craftsmanship: Facile and precise determination of oxygen reduction reaction activity by spraying catalyst ink on rotating disk electrode. Journal of Electroanalytical Chemistry. 2021;886.

[9] Lyu X, Van Cleve T, Young E, Li J, Yu H, Cullen DA, et al. Design of graded cathode catalyst layers with various ionomers for fuel cell application. Journal of Power Sources. 2023;556.

[10] Srivastav H, Weber AZ, Radke CJ. Colloidal Stability of PFSA-Ionomer Dispersions Part II: Determination of Suspension pH Using Single-Ion Potential Energies. Langmuir. 2024;40:6666-74.

[11] Kumano N, Kudo K, Akimoto Y, Ishii M, Nakamura H. Influence of ionomer adsorption on agglomerate structures in high-solid catalyst inks. Carbon. 2020;169:429-39.

[12] Liu P, Yang D, Li B, Zhang C, Ming P. Recent progress of catalyst ink for roll-to-roll manufacturing paired with slot die coating for proton exchange membrane fuel cells. International Journal of Hydrogen Energy. 2023;48: 19666-85.

[13] Hasegawa N, Kamiya A, Matsunaga T, Kitano N, Harada M. Analysis of crack formation during fuel cell catalyst ink drying process. Reduction of catalyst layer cracking by addition of high boiling point solvent. Colloids and Surfaces A: Physicochemical and Engineering Aspects. 2021;628.

[14] Welch C, Labouriau A, Hjelm R, Orler B, Johnston C, Kim YS. Nafion in Dilute Solvent Systems: Dispersion or Solution? ACS Macro Letters. 2012;1:1403-7.

[15] Ngo TT, Yu TL, Lin H-L. Influence of the composition of isopropyl alcohol/water mixture solvents in catalyst ink solutions on proton exchange membrane fuel cell performance. Journal of Power Sources. 2013;225:293-303.

[16] Li C, Yu K, Bird A, Guo F, Ilavsky J, Liu Y, et al. Unraveling the core of fuel cell performance: engineering the ionomer/catalyst interface. Energy & Environmental Science. 2023;16:2977-90.

[17] Li H, Zhao H, Jian S, Tao B, Gu S, Xu G, et al. Designing proton exchange membrane fuel cells with high specific power density. Journal of Materials Chemistry A. 2023;11:17373-91.